Physics of Plasmas

RESEARCH ARTICLE | APRIL 03 2024

Underwater electrical wire explosions under different discharge types: An experimental study with high initial energy storage

Shaojie Zhang ; Wansheng Chen; Yong Lu ; Yongmin Zhang; Shuangming Wang; Aici Qiu; Liang Ma; Liang Gao; Fei Chen

Phys. Plasmas 31, 043505 (2024)
https://doi.org/10.1063/5.0190438

Physics of Plasmas ARTICLE pubs.aip.org/aip/pop

Underwater electrical wire explosions under different discharge types: An experimental study with high initial energy storage

Cite as: Phys. Plasmas **31**, 043505 (2024); doi: 10.1063/5.0190438
Submitted: 6 December 2023 · Accepted: 22 March 2024 ·
Published Online: 3 April 2024

View Online Export Citation CrossMark

Shaojie Zhang,[1,a)] Wansheng Chen,[2] Yong Lu,[1] Yongmin Zhang,[1] Shuangming Wang,[1] Aici Qiu,[1] Liang Ma,[2] Liang Gao,[2] and Fei Chen[2]

AFFILIATIONS
[1]State Key Laboratory of Electrical Insulation and Power Equipment, Xi'an Jiaotong University, Xi'an 710049, China
[2]Shenmu Ningtiaota Mining Company Limited, Shaanxi Coal Group, Yulin 719314, China

[a)]Author to whom correspondence should be addressed: sjzhang2020@126.com

ABSTRACT

In this study, underwater electrical explosions of aluminum wires of various sizes were carried out with an initial energy storage of ∼53.5 kJ. Two piezoelectric probes were adopted to record the pressure waveforms. The experiments were divided into different discharge types, and the statistical properties of the electrical and shock-wave parameters of the different discharge types were compared. The experimental results show that there are three discharge types, called type A (breakdown type), type B (transition type), and type C (matched type). The three types differ in the resistance characteristics of the plasma channel during the plasma growth process, which are determined from the average electrical field strength and the remaining energy in the circuit at the peak voltage. Shock waves from type C discharges are more likely to exhibit a higher peak pressure, a larger impulse, and a higher energy density than the other types. However, using a matched wire that matches a specific discharge type, a high peak pressure, large impulse, and high energy density can also be achieved under type A or type B discharges. For example, the maximum peak pressures at ∼33 cm under type B and type C discharges are 38.7 and 42.4 MPa, respectively. These results provide significant guidance for load selection in underwater electrical wire explosion engineering applications.

I. INTRODUCTION

Electrical wire explosion (EWE) is a rapid phase transition process (including the melting, vaporization, and ionization) of a fine metal wire due to Joule heating by a high pulsed current.[1] EWE is accompanied by high-energy physical effects, such as pulsed electromagnetic radiation and shock waves (SWs), and has, therefore, attracted extensive attention from researchers.[2–7] Researchers have studied EWE for different purposes, including inertial confinement fusion,[8] warm dense matter,[9] nanoparticle synthesis,[10] electrohydraulic forming,[11] and reservoir stimulation.[7,12–14] EWE can occur in various media, including vacuum, air, water, etc. Underwater EWE (UEWE) generates stronger SWs[15,16] than EWE in air and has, thus, attracted extensive attention as a source of underwater SWs.

Conventionally, UEWEs with different circuit parameters or loads are classified into several discharge types depending on their voltage and current waveforms. The discharge types of EWEs in air were first summarized by Chace *et al.*[17] In recent decades, researchers have identified UEWE discharge types, including the current pause (dwell) type, breakdown type, and matched (optimal) type. In the current pause type, the phase transition and ionization processes are separated. Two SWs are generated and separated by a certain interval in time, and these are often used to study the physical mechanisms behind UEWEs.[18–20] In contrast, the discharges of the breakdown and matched types are continuous, and only one SW is generated. Among the three discharge types, the matched type is generally considered to have the highest electrical-to-mechanical energy conversion efficiency and to generate the strongest SWs.[21–25] Further detailed descriptions of the three discharge types can be found in Refs. 1 and 26. Han *et al.*[27] previously compared the characteristics (including the voltage, current, light intensity, and SWs) of the three discharge types. In terms of the SW peak pressure (of the first SW for the current pause type and the single SW for the others), the results indicated that the peak pressure increased from the current pause type to the breakdown type to the matched type from ∼2 MPa to more than ∼7.5 MPa. However, the experiments were carried out under a low initial energy (500 J) and used four types of wires with a fixed length (4 cm) and various diameters (50, 100, 200, and 300 μ m). The comparisons focused on the differences in the physical processes under different discharge types while ignoring the statistical differences in important parameters (e.g., whether the peak pressure of SWs under the matched type must be higher than that under the current pause and breakdown discharges regardless of the length and diameter of the wires). In addition, the initial energy storage in these experiments was too low to support the industrial applications of strong SWs, and the UEWE discharge types may differ with an initial energy storage of 500 J and tens of kilojoules. These limitations were also identified in the conclusions of other researchers.[28] It can be concluded that the current set of experimental results needs to be further enriched for a wide range of wire lengths and diameters and an initial energy storage of tens of kilojoules.

In this study, UEWEs with an initial energy storage of ~53.5 kJ were produced for various wire diameters and lengths. The experiments were divided into different discharge types according to the discharge current characteristics. Furthermore, the statistical properties of the electrical and SW parameters under different discharge types were compared. The results of this study are expected to help provide a better understanding of the physical process of UEWEs and to provide a reference for load selection in UEWE industrial applications.

II. EXPERIMENTAL SETUP

A layout of the experimental setup is shown in Fig. 1. A pulsed current supply was used with a peak energy storage of 195.3 kJ (a peak charging voltage of 30 kV), comprising two 217 μF capacitors connected in parallel and a gas spark switch. The output of the current supply was connected to a self-made coaxial component through a 29 m-long coaxial cable. The coaxial component was used to fix loads and was submerged in a stainless steel tank (ϕ 2000 × 1500 mm^2) filled with tap water.

A circuit diagram of the experimental setup is shown in Fig. 2. A transformer T was used to boost the output of an alternating current power VS and supply power to a 30 kV direct current power. The direct current power could generate a 0–30 kV voltage to charge the capacitors. Through 15.7 kV short-circuit discharges, the resistance R_0 and inductance L_0 of the discharge circuit and the R_t and L_t of the coaxial component were calculated to be 31.25 mΩ, 6.83 μH, 4.15 mΩ, and 265.70 nH, respectively. In the short-circuit discharges, the discharge period and peak current were 352.35 μs and 108.91 kA, respectively.

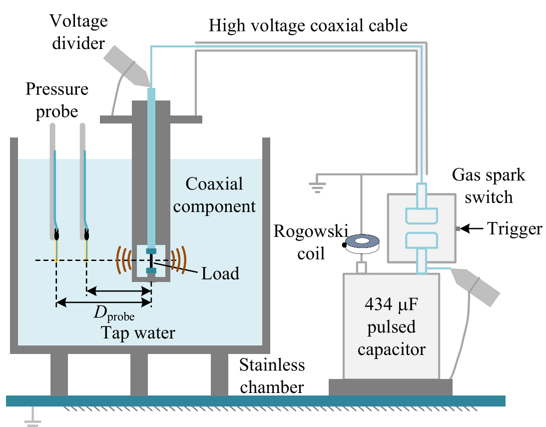

FIG. 1. A layout of the experimental setup.

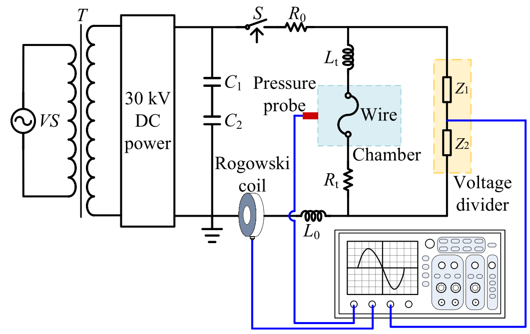

FIG. 2. A circuit diagram of the experimental setup.

The voltage drop on the coaxial component with a load was measured using a PVM-1 voltage divider (with a bandwidth of 120 MHz) from North Star. The current waveform was obtained with a CWT 1500 current coil placed around the cathode (with a bandwidth range of 0.03 Hz to 16 MHz) from Power Electronic Measurements. The resistive voltage u_R of the load can be calculated as

$$u_R(t) \approx u(t) - (L_w + L_t)\frac{di(t)}{dt} - R_t i(t),$$

where $u(t)$ is the voltage measured using the PVM-1, $i(t)$ is the circuit current, and L_w is the load inductance. The load voltages discussed below are resistive voltages.

The waveforms of the SWs generated by the UEWEs were measured with two commercial PCB138A11 probes (with a bandwidth range of 2.5 Hz to 1 MHz) from PCB Piezotronics. The two probes were mounted at distances of ~33 and ~49 cm from the load. The sensitive elements were maintained at the load center. Signals from all diagnostics were recorded using Tektronix Oscilloscopes MDO3054 and DPO4104B.

In this study, aluminum wires with diameters of 1.2, 1.6, 1.8, and 2.0 mm and lengths of 6, 8, 10, and 12 cm were selected to be exploded in water with an initial energy storage of ~53.5 kJ. The mass and E_{atom} values of all loads are listed in Table I, where E_{atom} refers to the energy required to heat a wire from room temperature to boiling temperature and complete atomization under atmospheric pressure. The skin depth was calculated according to the discharge period of the short-circuit experiment to be 1.538 mm (aluminum, 2.838 kHz), so the skin effect is not considered in the subsequent analysis.

III. DISCHARGE-TYPE CHARACTERISTICS

The current waveforms of the UEWEs are displayed in Fig. 3 for two cases representing different waveforms in repeatable experiments. The discharge types for all cases are also presented in Fig. 3. Type A and type C represent the breakdown and matched types,[1,26] respectively. Type B is a transition type between type A and type C. The current pause mode is not included due to the demand for strong SWs. Detailed descriptions of the three types are provided as follows:

TABLE I. The masses and E_{atom} values of wires with various diameters and lengths.

Number	Length (cm)	Diameter (mm)	Mass (g)	E_{atom} (kJ)	Number	Length (cm)	Diameter (mm)	Mass (g)	E_{atom} (kJ)
#1		1.2	0.18	2.47	#9		1.2	0.31	4.11
#2		1.6	0.33	4.38	#10		1.6	0.54	7.31
#3	6	1.8	0.41	5.55	#11	10	1.8	0.69	9.25
#4		2.0	0.51	6.85	#12		2.0	0.85	11.42
#5		1.2	0.24	3.29	#13		1.2	0.37	4.93
#6		1.6	0.43	5.85	#14		1.6	0.65	8.77
#7	8	1.8	0.55	7.40	#15	12	1.8	0.82	11.10
#8		2.0	0.68	9.13	#16		2.0	1.02	13.70

(1) Type A: The wire undergoes the phase transition, and the vapor-drop mixture is then ionized and converted into plasma. The remaining energy in the circuit is dissipated with a fixed period of underdamped discharge. The three typical type A current waveforms are called types A-1, A-2, and A-3 and are distinct from each other in terms of their current trends after ionization. The current increases again under type A-1, and the absolute maximum value is attained. The current increases again under type A-2, but only the local maximum value is observed. The current decreases under type A-3. Generally, the UEWE discharge type for a thin and short wire is type A-1. For a thin and long wire, it is type A-2, and for other intermediate sizes, it is type A-3.
(2) Type B: The remaining energy in the circuit is consumed by an underdamped discharge with a non-fixed period after ionization; i.e., the underdamped discharge exhibits different periods before and after the first zero-crossing point of the current.
(3) Type C: After ionization, the remaining energy in the circuit is dissipated as an underdamped discharge until the first zero-crossing point of the current is reached. Then the current is cut off. Type C includes two typical current waveforms, identified as types C-1 and C-2, which differ in whether the current strikes again. The current was completely cut off under type C-1, but under type C-2, it could strike again as the explosion products expanded.

The three discharge types are distinguished by their current behaviors during the plasma growth process, especially after the first zero-crossing of the current. It is well known that the current behavior is related to the peak voltage and the remaining energy in the circuit at peak voltage because these two parameters influence the development of electron avalanches and the resistance characteristics of the discharge plasma channel. If the peak voltage and the remaining energy are sufficient to transfer the low-ionized, high-resistance vapor-drop mixture to the plasma channel with higher conductivity, the remaining energy is dissipated with a fixed period of underdamped discharge (type A). On the contrary, if the peak voltage or the remaining energy is insufficient, the plasma channel has low conductivity, which causes the plasma channel to be partially closed (type B) or completely closed (type C) at the first zero-crossing point of the current.

The parameter E_{avg} is introduced to define the average electrical field strength of the discharge channel at peak voltage and is calculated by dividing the peak voltage by the wire length. The parameters E_1 and E_1^0 are also introduced to define the energy deposited on a wire and dissipated in the external circuit from the beginning of the discharge to the voltage peak, respectively. The remaining energy E_1^r in the circuit at peak voltage can be calculated by subtracting E_1 and E_1^0 from E_0, where E_0 is the initial stored energy of ∼53.5 kJ. Table II lists the peak voltage, E_{avg}, E_1, E_1^0, E_1^r, and discharge types for various UEWEs. As the wire diameter increased at a given length, the peak voltage decreased, while E_1 and E_1^0 increased, resulting in both E_{avg} and E_1^r decreasing and accordingly, the discharge type gradually changing from type A to type B to type C. As the wire length increased at a certain diameter, the peak voltage increased while E_{avg} did not increase significantly. In addition, E_1 increased while E_1^0 remained almost constant, resulting in a decreasing E_1^r. As a result, the discharge type also gradually changed from type A to type B to type C.

The relationship between the discharge types and the wire mass can also be analyzed. The discharge types for various UEWEs with different masses are summarized in Table III. As is evident, the discharge type gradually changed from type A to type B to type C with an increase in the wire mass. In addition, the transitions between the different discharge types were ambiguous. The relationship between the discharge types and the wire mass may be related to the ratios of E_0/E_{atom}, which are also listed in Table III. It is found that when E_0/E_{atom} was less than ∼6, the discharge was critically damped (type C). However, the physical mechanisms behind this relationship are still unclear and require further study.

IV. STATISTICAL PROPERTIES OF THE ELECTRICAL AND SHOCK-WAVE PARAMETERS

It is clear from the above-mentioned analysis that the discharge type changes as the wire size changes. Therefore, it is not rigorous to compare the characteristics of UEWEs under different discharge types by fixing the length or diameter and changing the other. Comparisons should be made using statistical methods over a wide range of wire lengths and diameters.

A. Electrical parameters

The parameter E_2 is defined as the energy deposited into a wire from the voltage peak to the first zero-crossing of the current. It describes the energy injection during the plasma growth process. The total energy deposition during the first half of the discharge cycle is represented by E. The parameter E_v is also introduced to define the energy deposition from the decrease in the current to the voltage peak (the main vaporization process), and it determines the rapid

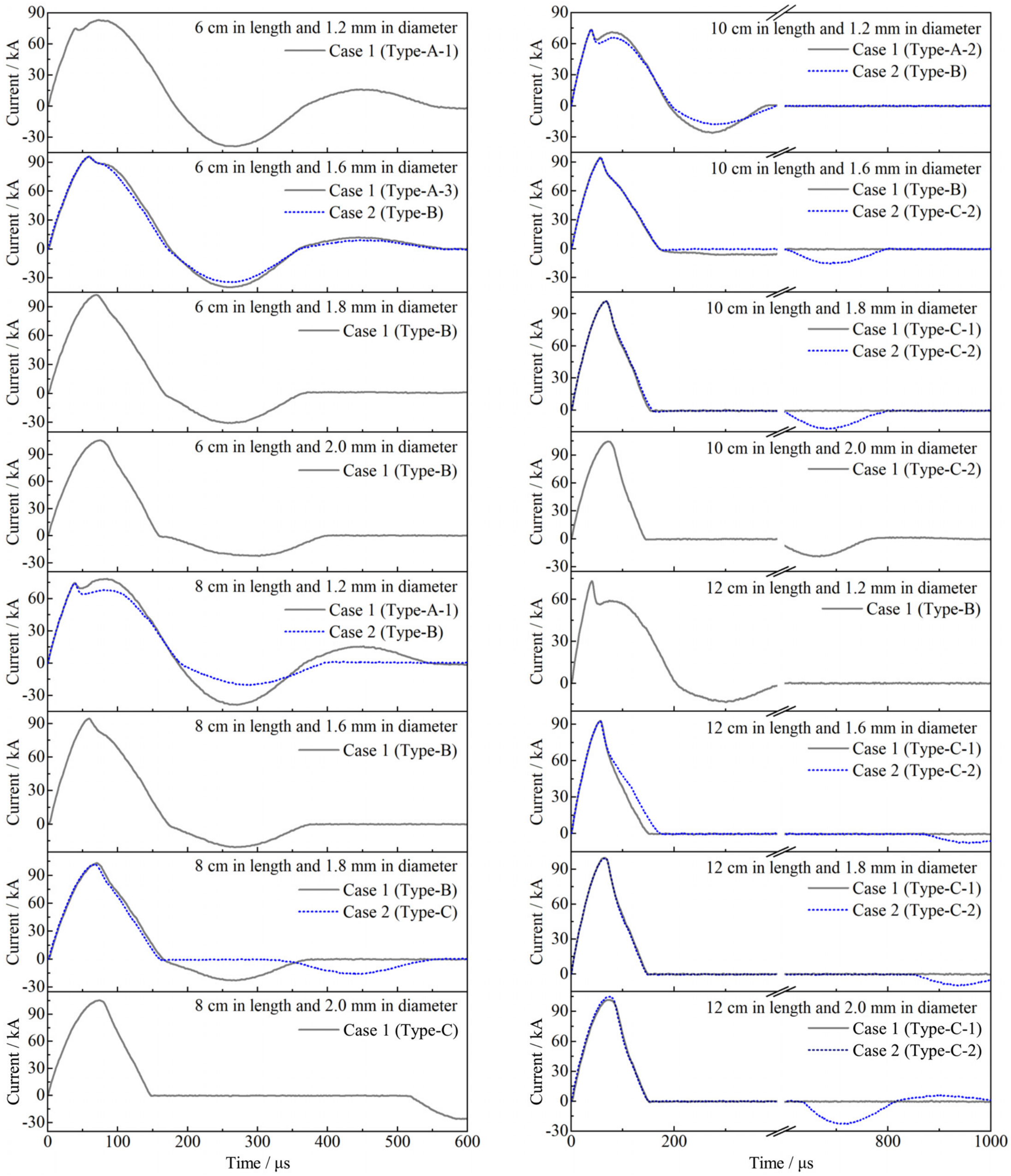

FIG. 3. Current waveforms of the UEWEs.

expansion of the discharge channel and SW generation.[29,30] The energy deposition parameters E_1, E_2, E, and E_v for UEWEs under different discharge types are presented in Fig. 4. Table IV lists the average values of the energy deposition parameters E_1, E_2, E, and E_v of the UEWEs under different discharge types. E_1 and E_v increased as the discharge types changed from type A to type C. This is due to E_1 and E_v mostly being related to the wire mass and the discharge types gradually changing from type A to type C with increasing wire mass. For E_2, there was no apparent advantage for UEWEs with different discharge types. This is because E_2 is related to the wire resistance but not the discharge type. For E, the average value increased slightly as the discharge types changed from type A to type C. However, explosions with high E were observed for UEWEs with different discharge types (37.3 kJ under type B and 39.6 kJ under type C). In other words, the values of E indicated no obvious advantage for UEWEs with different discharge types.

TABLE II. Peak voltages, E_{avg}, E_1, E_1^0, E_1^r, and discharge types of the UEWEs.

Number	Length (cm)	Diameter (mm)	Peak voltage (kV)	E_{avg} (kV/cm)	E_1 (kJ)	E_1^0 (kJ)	E_1^r (kJ)	Discharge type
#1	6	1.2	10.2 ± 0.06	1.70	3.2 ± 0.02	3.5 ± 0.07	46.8	A
#2		1.6	7.6 ± 0.31	1.27	3.9 ± 0.07	9.5 ± 0.16	40.1	A/B
#3		1.8	7.0 ± 0.23	1.17	7.2 ± 0.95	15.5 ± 0.70	30.8	B
#4		2.0	7.2 ± 0.01	1.21	7.6 ± 1.01	20.2 ± 0.70	25.7	B
#5	8	1.2	14.2 ± 0.04	1.77	4.3 ± 0.22	3.6 ± 0.09	45.6	A/B
#6		1.6	10.0 ± 0.17	1.25	5.9 ± 0.66	9.5 ± 0.28	38.1	B
#7		1.8	9.3 ± 0.94	1.17	8.5 ± 0.63	15.4 ± 0.90	29.6	B/C
#8		2.0	10.1 ± 0.59	1.27	9.1 ± 0.48	19.8 ± 0.58	24.6	C
#9	10	1.2	19.3 ± 1.29	1.93	5.5 ± 0.15	3.7 ± 0.01	44.3	A/B
#10		1.6	13.0 ± 0.28	1.30	7.7 ± 1.14	9.4 ± 0.57	36.4	B/C
#11		1.8	13.8 ± 0.51	1.38	10.4 ± 1.03	14.7 ± 0.81	28.4	C
#12		2.0	12.1 ± 0.66	1.21	7.9 ± 0.94	19.8 ± 0.32	25.8	C
#13	12	1.2	21.1 ± 0.08	1.76	6.2 ± 0.27	3.7 ± 0.02	43.6	B
#14		1.6	17.7 ± 0.76	1.47	10.4 ± 0.03	9.3 ± 0.24	33.8	C
#15		1.8	15.1 ± 0.41	1.26	10.7 ± 0.21	14.5 ± 0.41	28.3	C
#16		2.0	12.9 ± 0.51	1.08	12.8 ± 1.59	19.9 ± 0.41	20.8	C

TABLE III. Discharge types and ratios of E_0 to E_{atom} for various UEWEs.

Number	Mass (g)	Discharge type	E_0/E_{atom}	Number	Mass (g)	Discharge type	E_0/E_{atom}
#1	0.18	Type A	21.7	#5	0.24	Type A/B	16.3
#9	0.31	Type A/B	13.0	#2	0.33	Type A/B	12.2
#13	0.37	Type B	10.8	#3	0.41	Type B	9.6
#6	0.43	Type B	9.2	#4	0.51	Type B	7.8
#10	0.54	Type B/C	7.3	#7	0.55	Type B/C	7.2
#14	0.65	Type C	6.1	#8	0.68	Type C	5.9
#11	0.69	Type C	5.8	#15	0.82	Type C	4.8
#12	0.85	Type C	4.7	#16	1.02	Type C	3.9

The ratio of the energy deposition parameters E_1 to E_{atom} is introduced to evaluate the extent of vaporization of a wire at peak voltage. The ratios for UEWEs with different discharge types are shown in Fig. 5. The values of E_1/E_{atom} were less than 1.5 in all experiments and even less than 1 in some instances under type A/B and type C. The latter indicates that for an UEWE under pulsed discharge over hundreds of microseconds, the wire may not be completely vaporized at peak voltage when the initial energy storage is four times the value of E_{atom} or more. This may be due to thermal and magnetohydrodynamic instabilities.[31,32] Furthermore, the average values of the ratios under type C were slightly smaller than those under type A and type B.

B. Shock-wave parameters

The peak SW pressures generated by UEWEs under different discharge types are shown in Fig. 6. At a distance of ∼33 cm from the wire axis, the average peak pressure under type C was significantly higher than that under the other discharge types. However, this does not mean that every peak pressure under type C was greater than that under the other discharge types. For example, at ∼33 cm, the UEWEs under type B and type B/C could generate SWs with peak pressures as high as 38.7 and 34.2 MPa, respectively, which are smaller than only two of the six cases under type C. This indicates that each discharge type has a matched wire that matches that discharge type, in which case the UEWE can produce an SW with the highest peak pressure under that discharge type. Similarly, it can be seen from Fig. 6(b) that the peak pressures of SWs at ∼49 cm had the same tendency. In conclusion, by using a matched wire that matches a specific discharge type, an UEWE under each discharge type can generate an SW with a high peak pressure. Without limiting the wire size, an UEWE under type C is more likely to generate a SW with a higher peak pressure.

The impulses of SWs generated by UEWEs under different discharge types at ∼33 cm are illustrated in Fig. 7(a) and can be calculated using

$$J = \int_{t_{sp}}^{t_{ep}} p(t)\, dt, \tag{1}$$

where $p(t)$ is the time-varying pressure of the SW measured by the pressure probe at ∼33 cm, t_{sp} is the arrival time of the SW, and t_{ep} is

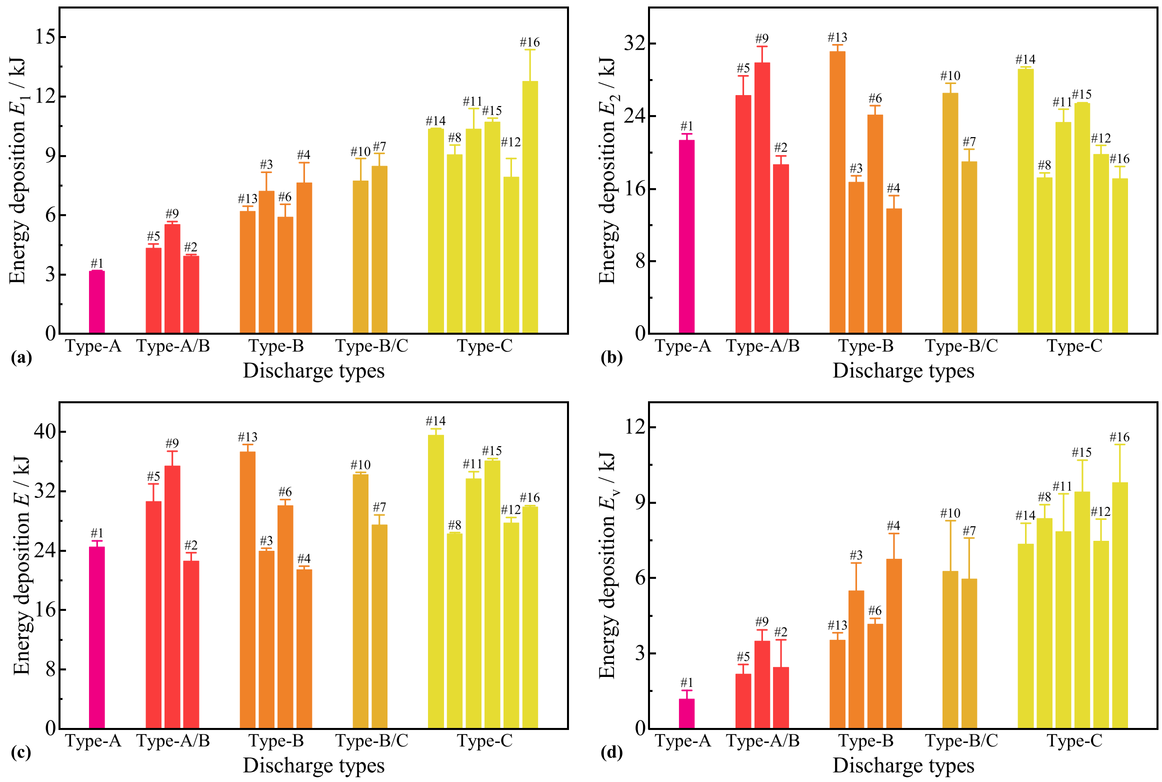

FIG. 4. The energy deposition parameters E_1 (a), E_2 (b), E (c), and E_v (d) for UEWEs with different discharge types. The wire mass corresponding to each data point increases from left to right, and the numbers are also labeled.

TABLE IV. The average values of the energy deposition E_1, E_2, E, and E_v for UEWEs under different discharge types.

Discharge type	E_1 (kJ)	E_2 (kJ)	E (kJ)	E_v (kJ)
Type A	3.17	21.35	24.52	1.18
Type A/B	4.60	24.95	29.55	2.71
Type B	6.74	21.46	28.20	4.99
Type B/C	8.11	22.77	30.88	6.12
Type C	10.19	22.02	32.21	8.38

700 μs after t_{sp}, at which point the SW pressure drops to a very low level. The energy densities of the SWs are shown in Fig. 7(b) and can be calculated using

$$w_p = \int_{t_{sp}}^{t_{ep}} \frac{p(t)^2}{\rho_0 c_0} dt, \quad (2)$$

where ρ_0 and c_0 are the density and sound velocity of undisturbed water, respectively. As expected, at $\sim$33 cm, the impulse and energy density of SWs under different discharge types have consistent laws with their peak pressure.

Generally, SWs under type C were more likely to exhibit a high peak pressure, large impulse, and high energy density than the other types. However, using a matched wire that matches a specific discharge type, a high peak pressure, large impulse, and high energy density can also be achieved under type A or B.

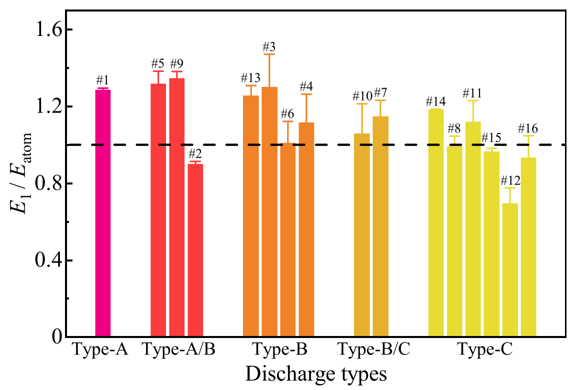

FIG. 5. The ratios of E_1 to E_{atom} for UEWEs with different discharge types.

V. CONCLUSION

In this study, we have conducted UEWEs of aluminum wires with an initial energy storage of approximately 53.5 kJ. The experimental results revealed three clear discharge types, called type A (breakdown type), type B (transition type), and type C (matched type).

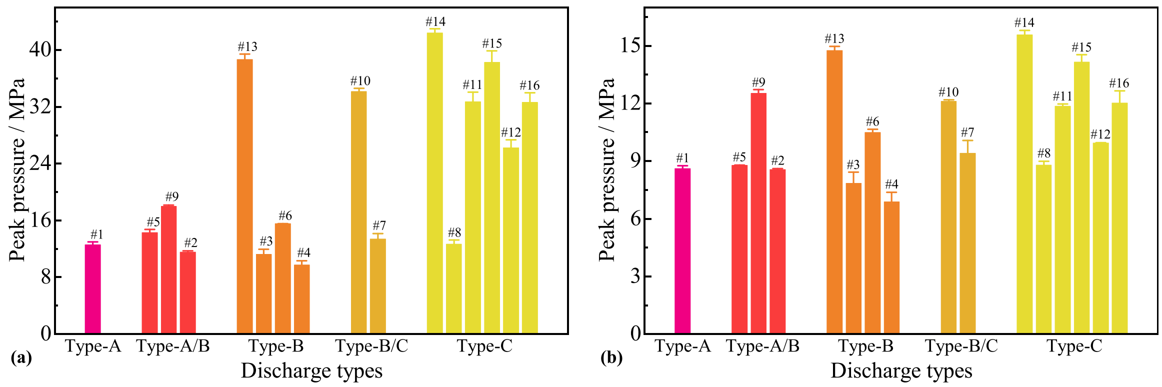

FIG. 6. The peak pressures of SWs generated by UEWEs under different discharge types at distances of ∼33 (a) and ∼49 cm (b) from the wire axis.

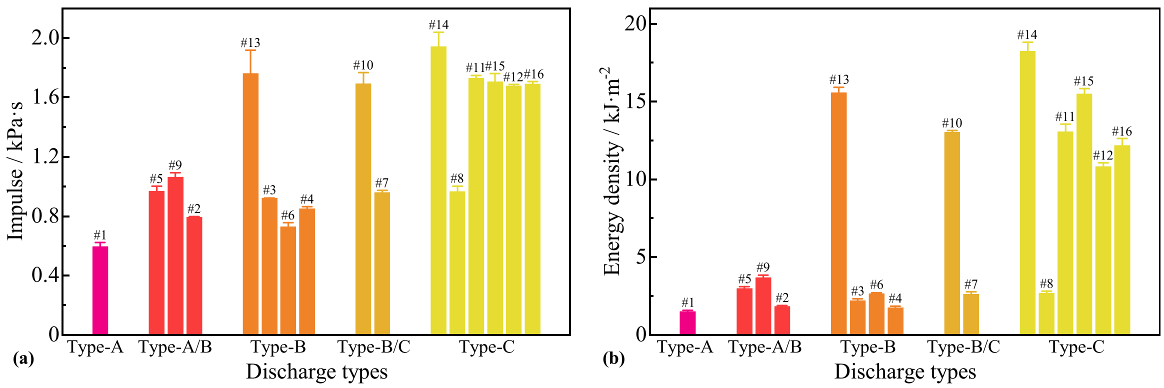

FIG. 7. The impulse (a) and energy density (b) of SWs generated by UEWEs under different discharge types at ∼33 cm.

The three discharge types are distinguished by the resistance characteristics of the discharge plasma channel during the plasma growth process, which is determined by the average electrical field strength and the remaining energy in the circuit at peak voltage. If the discharge plasma channel has higher conductivity, the discharge is type A; if not, it is type C. The discharge type gradually changed from type A to type B to type C as the wire diameter increased at a fixed length, as the length increased at a fixed diameter, or as the mass increased.

The energy deposition E_1 increased as the discharge types changed from type A to type C, as did E_v. For E_2 and E, however, there were no apparent advantages provided by different discharge types. In addition, the ratios of E_1 to E_{atom} indicate that for an UEWE under pulsed discharge over hundreds of microseconds, the wire may not be completely vaporized at peak voltage when the initial energy storage is four times E_{atom} or more.

Overall, SWs generated by UEWEs under type C were more likely to exhibit a high peak pressure, large impulse, and high energy density. Under type A or type B, a high peak pressure, large impulse, and high energy density could still be achieved using a matched wire that matched the discharge type. The results of this study aid in understanding the physical processes underlying UEWE and can act as an important guideline for load selection in UEWE engineering applications. However, there may be some limitations. As a result, further research will be conducted to understand these mechanisms in more detail.

ACKNOWLEDGMENTS

The authors express their gratitude to the reviewers for their detailed and valuable comments and suggestions. The authors also thank Ms. Yuan for her help with LaTeX writing.

AUTHOR DECLARATIONS

Conflict of Interest

The authors have no conflicts to disclose.

Author Contributions

Shaojie Zhang: Conceptualization (equal); Data curation (equal); Formal analysis (equal); Investigation (equal); Methodology (equal); Visualization (equal); Writing – original draft (equal); Writing – review & editing (equal). **Wansheng Chen:** Funding acquisition (equal); Resources (equal); Supervision (equal). **Yong Lu:** Investigation (equal); Software (equal); Supervision (equal); Validation (equal); Writing – review & editing (equal). **Yongmin Zhang:** Conceptualization (equal); Funding acquisition (equal); Project administration (equal); Resources (equal); Supervision (equal); Writing – review & editing (equal). **Shuangming Wang:** Funding acquisition (equal); Resources (equal); Supervision (equal). **Aici Qiu:** Funding acquisition (equal); Project administration (equal); Resources (equal); Supervision (equal). **Liang Ma:** Funding acquisition (equal); Resources (equal); Supervision (equal). **Liang Gao:** Funding acquisition (equal); Resources (equal); Supervision (equal). **Fei Chen:** Funding acquisition (equal); Resources (equal); Supervision (equal).

DATA AVAILABILITY

The data that support the findings of this study are available from the corresponding author upon reasonable request.

REFERENCES

[1] H. Shi, G. Yin, X. Li, J. Wu, A. B. Murphy, Y. Zhang, and A. Qiu, "Electrical wire explosion as a source of underwater shock waves," J. Phys. D **54**, 403001 (2021).
[2] A. Grinenko, V. T. Gurovich, A. Saypin, S. Efimov, Y. E. Krasik, and V. Oreshkin, "Strongly coupled copper plasma generated by underwater electrical wire explosion," Phys. Rev. E **72**, 066401 (2005).
[3] S. A. Pikuz, S. I. Tkachenko, V. M. Romanova, T. A. Shelkovenko, A. E. Ter-Oganesyan, and A. R. Mingaleev, "Maximum energy deposition during resistive stage and overvoltage at current driven nanosecond wire explosion," IEEE Trans. Plasma Sci. **34**, 2330–2335 (2006).
[4] A. Grinenko, Y. E. Krasik, S. Efimov, A. Fedotov, V. T. Gurovich, and V. I. Oreshkin, "Nanosecond time scale, high power electrical wire explosion in water," Phys. Plasmas **13**, 042701 (2006).
[5] Y. E. Krasik, A. Grinenko, A. Sayapin, S. Efimov, A. Fedotov, V. Z. Gurovich, and V. I. Oreshkin, "Underwater electrical wire explosion and its applications," IEEE Trans. Plasma Sci. **36**, 423–434 (2008).
[6] Y. E. Krasik, A. Fedotov, D. Sheftman, S. Efimov, A. Sayapin, V. T. Gurovich, D. Veksler, G. Bazalitski, S. Gleizer, A. Grinenko *et al.*, "Underwater electrical wire explosion," Plasma Sources Sci. Technol. **19**, 034020 (2010).
[7] R. Han, J. Wu, H. Zhou, Y. Zhang, A. Qiu, J. Yan, W. Ding, C. Li, C. Zhang, and J. Ouyang, "Experiments on the characteristics of underwater electrical wire explosions for reservoir stimulation," Matter Radiat. Extremes **5**, 047201 (2020).
[8] J. Wu, Y. Lu, F. Sun, X. Jiang, Z. Wang, D. Zhang, X. Li, and A. Qiu, "Researches on preconditioned wire array Z pinches in Xi'an Jiaotong University," Matter Radiat. Extremes **4**, 036201 (2019).
[9] M. Desjarlais, J. Kress, and L. Collins, "Electrical conductivity for warm, dense aluminum plasmas and liquids," Phys. Rev. E **66**, 025401 (2002).
[10] Y. A. Kotov, "Electric explosion of wires as a method for preparation of nanopowders," J. Nanopart. Res. **5**, 539–550 (2003).
[11] S. F. Golovashchenko, A. J. Gillard, and A. V. Mamutov, "Formability of dual phase steels in electrohydraulic forming," J. Mater. Process. Technol. **213**, 1191–1212 (2013).
[12] Y. Zhang, A. Qiu, H. Zhou, Q. Liu, J. Tang, and M. Liu, "Research progress in electrical explosion shockwave technology for developing fossil energy," High Vol. Eng. **42**, 1009–1017 (2016).
[13] Q. Liu, W. Ding, R. Han, J. Wu, Y. Jing, Y. Zhang, H. Zhou, and A. Qiu, "Fracturing effect of electrohydraulic shock waves generated by plasma-ignited energetic materials explosion," IEEE Trans. Plasma Sci. **45**, 423–431 (2017).
[14] Y. Hu, H. Shi, T. Li, Z. Tao, X. Li, J. Wu, Y. Zhang, and A. Qiu, "Underwater shock wave generated by exploding wire ignited energetic materials and its applications in reservoir stimulation," IEEE Trans. Plasma Sci. **50**, 2520–2527 (2022).
[15] G. S. Sarkisov, S. E. Rosenthal, K. R. Cochrane, K. W. Struve, C. Deeney, and D. H. McDaniel, "Nanosecond electrical explosion of thin aluminum wires in a vacuum: Experimental and computational investigations," Phys. Rev. E **71**, 046404 (2005).
[16] A. Grinenko, A. Sayapin, V. T. Gurovich, S. Efimov, J. Felsteiner, and Y. E. Krasik, "Underwater electrical explosion of a Cu wire," J. Appl. Phys. **97**, 023303 (2005).
[17] *Exploding Wires*, edited by W. G. Chace and H. K. Moore (Plenum Press, New York, 1959), Vol. 1.
[18] V. Romanova, A. Mingaleev, A. Ter-Oganesyan, T. Shelkovenko, G. Ivanenkov, and S. Pikuz, "Core structure and secondary breakdown of an exploding wire in the current-pause regime," Matter Radiat. Extremes **4**, 026401 (2019).
[19] H. Shi, G. Yin, Y. Fan, J. Wu, X. Li, and A. B. Murphy, "Multilayer weak shocks generated by restrike during underwater electrical explosion of Cu wires," Appl. Phys. Lett. **115**, 084101 (2019).
[20] S. I. Tkachenko, V. M. Romanova, T. A. Shelkovenko, A. E. Ter-Oganesyan, A. R. Mingaleev, and S. A. Pikuz, "Laser imaging of secondary breakdown upon nanosecond electrical explosion of wire," IEEE Trans. Plasma Sci. **36**, 1292–1293 (2008).
[21] T. Tobe, M. Kato, and H. Obara, "Energy consumption at underwater exploding-wire gap in electric discharge metal forming," Bull. JSME **21**, 1780–1786 (1978).
[22] T. Suhara and S. Fukuda, "Experimental determination of optimum condition for wire explosion in water and PMMA," Proc. SPIE **0819**, 321 (1979).
[23] S. Khainatskii, "Conditions for realization of an optimum regime of the electric explosion of conductors in liquid media," Tech. Phys. Lett. **35**, 299–301 (2009).
[24] N. Kuskova, V. Y. Baklar', and S. Khainatskii, "On obtaining of ultrafine metal powders under electric explosion of conductors in a liquid. Part II: The optimum mode for the explosion of conductors in a liquid," Surf. Eng. Appl. Electrochem. **45**, 186–192 (2009).
[25] A. Rososhek, S. Efimov, A. Virozub, D. Maler, and Y. E. Krasik, "Particularities of shocks generated by underwater electrical explosions of a single wire and wire arrays," Appl. Phys. Lett. **115**, 074101 (2019).
[26] X. Wang, "Research at Tsinghua University on electrical explosions of wires," Matter Radiat. Extremes **4**, 017201 (2019).
[27] R. Han, J. Wu, H. Zhou, W. Ding, A. Qiu, T. Clayson, Y. Wang, and H. Ren, "Characteristics of exploding metal wires in water with three discharge types," J. Appl. Phys. **122**, 033302 (2017).
[28] L. Li, D. Qian, X. Zou, and X. Wang, "Effect of deposition energy on underwater electrical wire explosion," IEEE Trans. Plasma Sci. **46**, 3444–3449 (2018).
[29] R. Han, H. Zhou, J. Wu, A. Qiu, W. Ding, and Y. Zhang, "Relationship between energy deposition and shock wave phenomenon in an underwater electrical wire explosion," Phys. Plasmas **24**, 093506 (2017).
[30] R. Han, H. Zhou, J. Wu, T. Clayson, H. Ren, J. Wu, Y. Zhang, and A. Qiu, "Experimental verification of the vaporization's contribution to the shock waves generated by underwater electrical wire explosion under micro-second timescale pulsed discharge," Phys. Plasmas **24**, 063511 (2017).
[31] V. I. Oreshkin, "Thermal instability during an electrical wire explosion," Phys. Plasmas **15**, 092103 (2008).
[32] S. Lebedev, I. Mitchell, R. Aliaga-Rossel, S. Bland, J. Chittenden, A. Dangor, and M. Haines, "Azimuthal structure and global instability in the implosion phase of wire array *Z*-pinch experiments," Phys. Rev. Lett. **81**, 4152 (1998).